ARCHIVES OF METALLURGY AND MATERIALS
Volume 52 2007 Issue 2

J. GAWĄD*, M. PIETRZYK*

APPLICATION OF CAFE MULTISCALE MODEL TO DESCRIPTION OF MICROSTRUCTURE DEVELOPMENT DURING DYNAMIC RECRYSTALLIZATION

ZASTOSOWANIE WIELOSKALOWEGO MODELU CAFE DO OPISU ROZWOJU MIKROSTRUKTURY W TRAKCIE DYNAMICZNEJ REKRYSTALIZACJI

Multiscale CAFE (Cellular Automata – Finite Element) model of the material undergoing dynamic recrystallization is presented in the paper. The coupled model consists of dislocation and microstructure development description based on Cellular Automata (CA) and continuum macroscale simulation using Finite Element (FE) method. The model is capable of simulate various characteristics of the material, including multi-peak and single-peak flow stress behaviour. Several improvements to the CA model are proposed in the paper. The connection between flow stress characteristic and grain size is properly described by the model with respect to the structural criterion. Additionally, distribution of grain size can be calculated at arbitrary stage of the process. Analysis of recrystallization cycles observed in the material is discussed. The results show good qualitative agreement with the experimental flow stress curves commonly observed in literature.

Keywords: Cellular automata, Dynamic recrystallization, Multiscale, CAFE, micro-macro analysis

W artykule zaprezentowano wieloskalowy model CAFE (Cellular Automata – Finite Element). Model ten złożony jest z symulacji rozwoju mikrostruktury i gęstości dyslokacji, opartej o metodę Automatów Komórkowych (AK, CA) oraz modelu skali makro, opartego o Metodę Elementów Skończonych (MES, FE). Zaproponowano szereg usprawnień do modelu skali mikro. Model ten umożliwia uwzględnienie różnych charakterystyk naprężenia uplastyczniającego, w tym jednopikowego i wielopikowego. Model poprawnie odwzorowuje kryterium strukturalne, łączące charakter krzywej naprężenia uplastyczniającego z wielkością ziarna. Zaletą modelu jest dostarczanie zarówno informacji o średniej wielkości ziarna jak i o rozkładzie wielkości. W pracy przeanalizowano krzywe opisujące ułamki cykli rekrystalizacji w materiale. Uzyskane z modelu krzywe naprężenia uplastyczniającego wykazuje dobrą zgodność jakościową z powszechnie znanymi z literatury danymi doświadczalnymi.

1. Introduction

Despite years of research, the unified theory of recrystallization is debatable, especially for dynamic recrystallization (DRX). The efforts which were made by experimentalist explained basic aspects of the DRX, including nucleation and grain growth. However, these results are often difficult to apply in simulation models. The expectations for realistic model of DRX encompass microstructure evolution as well as mechanical behaviour of the material. Among various approaches proposed for simulation of recrystallization, the most notable are Monte-Carlo Pott's method, Vertex Method and Cellular Automata. Review of these methods is presented in [1, 2]. Aforementioned methods take into account topology of the microstructure and its influence on primary grain boundary (GB) migration, nucleation of new grains and subsequent grain growth. However, these methods are proved useful only for small pieces of material, composed of up to thousands of grains. Another limitation is connected with the common assumption of constant temperature, strain rate and strain increments. These simplifications are unacceptable for larger samples, even for those used in the standard uniaxial compression tests.

Another group of models is aimed at coupling with solution of partial differential equations describing thermo-mechanical behaviour of the material. The finite element (FE) method is commonly used for this class of problems. However, treating the material as continuum is one of obstacles in the development of reliable DRX models. The FE models based on crystal plasticity theo-

* DEPARTMENT OF APPLIED COMPUTER SCIENCE AND MODELLING, FACULTY OF METALS ENGINEERING AND INDUSTRIAL COMPUTER SCIENCE, AGH UNIVERSITY OF SCIENCE AND TECHNOLOGY, 30-059 KRAKÓW, AL. MICKIEWICZA 30, POLAND

ry (CP-FEM) are able to cope with direct simulation of microstructure development, because every grain in the material is discretized by several finite elements. The fields of mechanical and thermal properties can be calculated. These methods are also limited to small pieces of material due to huge computational outlay, which is the main drawback of the methods. The Internal Variable Method (IVM) [3] coupled with FE is another approach to simulation of microstructure development. The method introduces a state variable, which represents state of the material and is usually connected with dislocation density. The multi-variable models were also proposed (e.g. [4]), where other parameters of microstructure are considered, such as an average subgrain size and the average misorientation angle between subgrains. Ability to account for the history of deformation is an advantage of IVM. One of the limitations of the IVM is lack of deep insight into phenomena of microstructure evolution, because the method operates on statistical level and neglects topological relationships in the microstructure. Obviously, the useful information about microstructure characteristics, such as mean grain size, is given. Alas, description of the material in a statistical manner reduces physical support, which is present in the previously discussed group of the methods.

Generally, the FE models of hot working processes in which DRX plays an important role, are mostly reliable and well-established even for industrial problems, but they suffer from the lack of the microstructural information. On the other hand, the CA and other methods of microstructure simulation can provide useful information about the material in microscale [1,5-11], but are limited to very small size of simulation domain. Moreover, complicated shapes of the sample are usually unacceptable for these methods. Therefore, the objective of the present work is to overcome those limitations by connection of the CA microstructural model with the FE macroscale simulation. The similar approaches are presented in [12, 13]. The emphasis in this work is put on development the transition rules, which give realistic description of phenomena occurring during dynamic recrystallization.

2. The CAFE model

The idea of the CAFE model is to couple FEM with physically supported CA simulation of material undergoing DRX. Therefore, the microscale and macroscale behaviour of the material is simulated by different methods, appropriate for respective scales. The CAFE model supplies information, which is hard to obtain using the pure CA or FE approach. Since the state of the material is hold within CA simulations and its changes determine the plastic flow, the model can be interpreted as an extended IVM. Moreover, while only a few scalars describe material state in the classic IVM, the image of microstructure is stored in the CAFE approach.

The uniaxial compression test is used as an example of the hot working process in this work. The CAFE model consists of three layers, which are shown in Fig. 1.

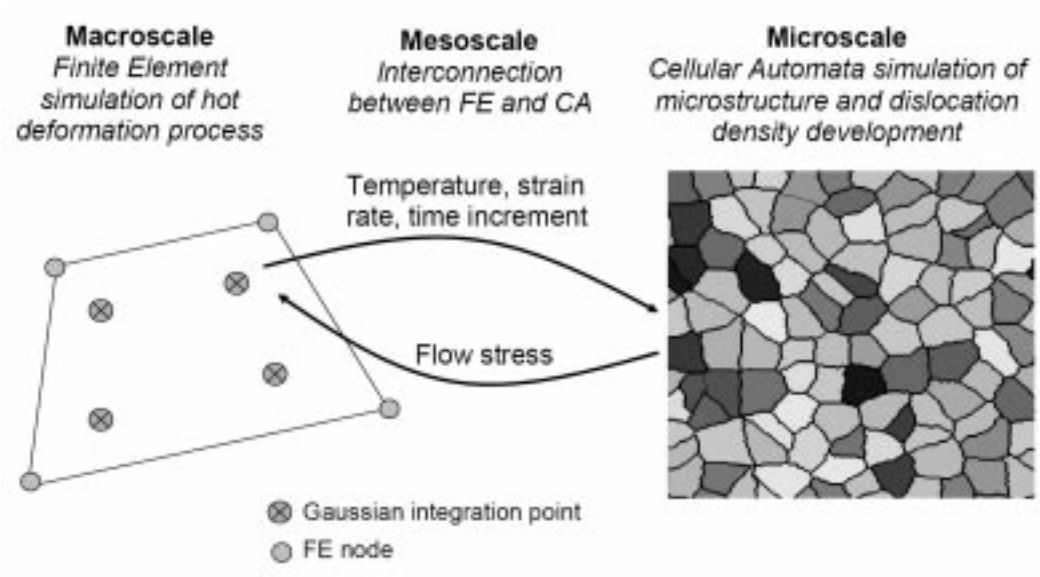

Fig. 1. The general concept of the presented CAFE solution

The first layer based on FEM is responsible for macroscopic description of the material. The second layer is used for interconnection between macroscopic and microscopic model, which include calculation of material parameters crucial for FE solution. The role of the third layer, which is based on CA calculations, is to simulate development of the microstructure and evolution of dislocation density. The mutual feedback between adjacent layers is introduced. Every Gauss integration point in the FE mesh is connected with separate microscale simulation through mesoscale model, which calculates flow stress on the basis of average dislocation density in CA lattice. The evolution of dislocation density and microstructure is governed by state transition rules of CA.

The software was developed, which allows agglomeration of quantities to be calculated at all levels of the model. The grain size can be mapped to the finite element mesh and postprocessed.

2.1. The macroscale FE model

The macroscopic layer describes the material behaviour as continuum, which includes calculation of strain, stress and strain rate and temperature fields. The flow formulation is used in the FE solution. This approach is based on the variational principle [14]:

$$\int_{\Omega} \sigma_{ij}^{'} \dot{\varepsilon}_{ij} d\Omega + \int_{\Omega} \lambda \dot{\varepsilon}_V d\Omega - \int_{\Gamma} \tau_i v_i d\Gamma = 0, \qquad (1)$$

where Ω – control volume, Γ – boundary of control volume, σ_{ij} – Cauchy tensor of stresses, $\dot{\varepsilon}_{ij}$ – strain rate tensor, v_i – velocity, λ – Lagrange multiplier. The incompressibility constraint is given by $\dot{\varepsilon}_V = 0$ in Ω, where $\dot{\varepsilon}_V$ – volumetric strain rate. The boundary conditions $\sigma_{ij} n_j = \tau_i$ on Γ_τ (suppressible boundary condition) and $\delta v_i = 0$ on Γ_v (essential boundary condition), are imposed.

In the flow theory of plasticity, strain rates are related to stresses by the Levy-Mises flow rule:

$$\underline{\boldsymbol{\sigma}} = \frac{2\sigma_f}{3\dot{\varepsilon}_{eff}} \underline{\dot{\boldsymbol{\varepsilon}}}, \qquad (2)$$

where $\underline{\boldsymbol{\sigma}}, \underline{\dot{\boldsymbol{\varepsilon}}}$ are the vectors containing components of stress and strain rate tensors, respectively, $\dot{\varepsilon}_{eff}$ – effective strain rate and σ_f – flow stress.

The mechanical problem is coupled with the FE solution of Fourier heat transfer equation:

$$\nabla \left[k(T) \nabla T \right] + Q(T) = c_p(T) \rho(T) \frac{\partial T}{\partial t}, \qquad (3)$$

where $k(T)$ – conductivity, T – temperature, $Q(T)$ – heat generated due to plastic work, $\rho(T)$ – density, $c_p(T)$ – specific heat, t - time. The boundary condition is prescribed at the boundary surface and it is a function of surface temperature of the workpiece, time and position:

$$k \frac{\partial T}{\partial \mathbf{n}} = q + \alpha (T - T_0), \qquad (4)$$

where $\mathbf{n}$ – unit vector normal to the surface, q – heat generated at the boundary, T – surface temperature, α – heat transfer coefficient, T_0 – temperature of the surrounding medium.

Discretization of functional (1) is performed using four node quadrilateral elements. The resulting set of non-linear equations is solved by the Newton-Raphson method. The detailed description of a thermal-mechanical FEM code developed by the authors is presented in [14].

2.2. Mesoscopic model

Since flow stress σ_f is the only material parameter in the flow rule (2), it is convenient to formulate intermediate model between CA and FE, which is responsible for calculation of σ_f. The link between macroscale and mesoscale model is similar to those used in the IVM. Contrary to the IVM, the present approach includes state variable, which has a complex structure and consists mainly of CA lattice and several auxiliary objects, including the simplified representation of grains in the microstructure. Thus, every Gauss integration point in the FE mesh is connected with the CA lattice and the flow stress is calculated by mesoscopic model in these points during each time increment of the FE solution. The local strain, strain rate, temperature and time increment provided by FE are passed to the corresponding CA lattice. The material response, calculated on the basis of dislocation density evolution in the CA space, is returned as a feedback to the FE code. Due to incompatibility of the time step lengths in the CA and FE simulations, the necessary interpolation of σ_f is performed. The flow stress is calculated as:

$$\sigma_f = \alpha \mu b \sqrt{\rho}_{avr}, \qquad (5)$$

where α – coefficient, μ – shear modulus, b – length of the Burger's vector, ρ_{avr} – average dislocation density in the CA lattice.

The mapping function between FE nodes and CA lattices enables assignment of different initial microstructures to each node. Each initial microstructure can be characterized by different distribution of grain size and orientation, as well as initial dislocation density. This feature is advantageous e.g. in case of simulation

which is performed for the samples of heterogeneous distribution of grain size. Moreover, smaller CA lattices can be assigned to the regions of material that are known to be subjected to smaller deformation.

2.3. Microscale CA model

The microscale CA model is responsible for the evolution of grain size and dislocation density. For this purpose the 2D CA lattice with periodic boundary conditions is used. The lattice of cells represents the image of microstructure and reproduces topological relations between grains. The state of each cell is represented by four state variables: (1) local dislocation density ρ, (2) orientation ϕ, (3) distance variable x that controls GB migration, (4) assignment of the cell to the grain. Additionally, the changes of grain assignment and other transitions of the state, which are concomitant with recrystallization in cells, are counted by auxiliary state variables, described further in the paper.

The image of initial microstructure is a starting point for calculations. This initial microstructure is generated using CA algorithm of a normal grain growth, partially based on the work [15]. The algorithm is adapted to the construction of the microstructure images with various distribution of grain size and orientation. Homogeneous distribution of the dislocation density ρ in the initial CA lattice is enforced. Example of generated microstructures is presented in Fig. 1.

Two kinds of neighbourhood are defined in the presented CA model. The first is based on Moore neighbourhood and modified in similar way as proposed in [16]. Two diagonal members of the neighbourhood are removed in a random manner. In consequence, the central cell is always surrounded by six neighbours leading to the pseudo-hexagonal neighbourhood (Fig. 2) [10]. This neighbourhood was selected to obtain globular shapes of growing nuclei due to reduction in influence of neighbourhood shape and the anisotropy of the CA lattice. For similar reasons the random factor was applied by other researchers (e.g. [6-9]), but rather incorporated into transition rules.

The second type of neighbourhood, called "Distant Neighborhood" (DN), is more sophisticated. It has features not typical of the standard CA neighbourhoods. The state of cells in the DN is not accessed directly by the cells belonging to, but is presented to them as an average value. The DN has its own internal state, which includes average orientation and average dislocation density. The number of cells in DN, denoted by n_{gr}, may change in time. If $n_{gr} > 0$ then DN persists, otherwise it disappears. Finally, the DN has no arbitrary topology and it changes when the cells are attached to or detached from the DN. The concept of DN, which represents grains in the model, assumes interactions of longer range than pseudo-hexagonal neighbourhood diameter. The interactions include migration of dislocations and are connected with mean free path of dislocations, which in turn depends on the subgrain size. It is assumed in the model that, for small recrystallized grains, the mean free path is comparable with the grain size:

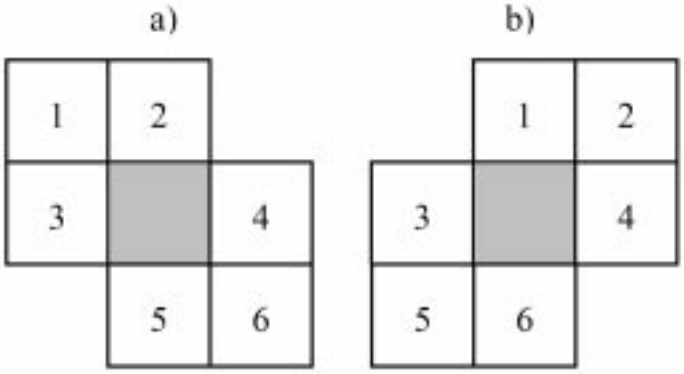

Fig. 2. The pseudo-hexagonal neighbourhood. The central cell (gray) is surrounded by six neighbours (numbered squares), which are selected by removal of random diagonal from Moore neighborhood. a) the right diagonal removed, b) the left diagonal removed

$$D = 2\sqrt{\frac{n_{gr}S_c}{\pi}}, \tag{6}$$

where D – substitute grain size, S_c – area of CA cell in DN. Non-uniform distribution of dislocation density is another motivation for DN concept. The increment of mean dislocation density is calculated at grain level, separately for each grain, using differential equation [17]:

$$\frac{d\rho_{gr}}{dt} = A - B\rho_{gr}, \tag{7}$$

where t – time, ρ_{gr} – average dislocation density within the grain, $A = \frac{\dot{\varepsilon}}{bl}$ and $B = k_{20}\dot{\varepsilon}^m \exp\left(\frac{Q_s}{RT}\right)$ – parameters pertaining to hardening and dynamic recovery, respectively, $\dot{\varepsilon}$ – strain rate, Q_s – activation energy of self-diffusion, b – length of Burger's vector, T – temperature, R – gas constant, k_{20}, m – parameters.

The average dislocation density calculated in a previous time step is used as an initial condition for solution of equation (7). The dislocation density in the cells belonging to the grain is then updated using random function. Therefore, a nonuniform distribution of the dislocation density within the CA lattice is obtained in turn. It should be noted, however, that all interactions between the cells remain local, i.e. there is still no global data required for transition of the state.

The construction of state transition rules is decisive for CA simulations. These rules have to enable simulation of two components of recrystallization: nucleation

and subsequent grain growth. The transition rules approximate the idea of DRX given in [18]. Despite the rules itself are deterministic, the result of their application is not deterministic due to quasi-random neighbourhood definition and distribution of dislocation density in the CA lattice. Substantially, there are two transition rules in the model. The first describes the nucleation and is based on critical dislocation density criterion. The rule states that the nucleus appears if the cell is located at GB and dislocation density in the cell reaches critical value ρ_c, given by the equation [19, 6]:

$$\rho_c = \left(\frac{20\gamma\dot{\varepsilon}}{3blM\tau^2}\right)^{1/3}, \tag{8}$$

where γ – grain boundary energy, $\dot{\varepsilon}$ – strain rate, M – grain boundary mobility, l – mean free path of dislocations, τ – average energy of dislocation line, b – length of Burger's vector.

Due to nonuniform distribution of dislocation density in grains, the value of ρ at the grain boundaries is also nonuniform. Thus, it is possible to select the subset of the sites in the CA lattice, in which the nuclei occur. Such formulation requires neither calculation of the nucleation probability nor nucleation rate, which is advantage in comparison to the previous approaches. It is assumed in the model that the random orientation is assigned to newly created nuclei. The dislocation density in the cell that becomes nucleus is set to ρ_{DRX}. Because each grain is identified with a distant neighbourhood, new DN is also created.

The second rule describes growth of recrystallized grains. The rules that control grain growth are based on calculation of velocity of GB motion v, which depends on GB mobility M and the driving force for growth F:

$$v = \alpha MF, \tag{9}$$

where α is the scaling factor. The GB mobility is calculated from Shvindlermann equation [20]:

$$M = M_m\left[1 - \exp\left(-B\frac{\theta}{\theta_m}\right)^n\right], \tag{10}$$

where θ – misorientation angle, M_m and θ_m are mobility for high angle boundary and the misorientation angle for high angle grain boundary, respectively, B, n – coefficients. The temperature dependence of the GB mobility is given by [21]:

$$M_m = M_0\exp\left(\frac{-Q}{kT}\right), \tag{11}$$

where M_0 – constant, Q – activation enthalpy for GB motion, k – Boltzmann constant, T – temperature. GB energy is calculated from the Read-Shockley equation [20]:

$$\gamma = \gamma_m\frac{\theta}{\theta_m}\left(1 - \ln\frac{\theta}{\theta_m}\right), \tag{12}$$

where γ_m – GB energy for high misorientation angle θ_m.

The relationship describing driving force for grain growth is derived from the work [6]. The main part of driving force is connected with difference in dislocation density between the current CA cell belonging to the recrystallized grain and the neighbouring cells belonging to the deformed matrix ρ_i:

$$F = \pi D^2\tau\,(\rho_i - \rho) - 4\pi D\gamma_i. \tag{13}$$

The substitute grain size D is calculated from equation (6). The distance variable x increment is evaluated from the GB velocity:

$$\Delta x = \frac{v\Delta t}{S}, \tag{14}$$

where Δt – length of the time step, S – actual area of the cell. The recrystallized volume fraction x_{rec} is updated by Δx using threshold function, which ensures $x_{\text{rec}} \leqslant 1$. The largest Δx is used for estimation of the time step in the CA simulation. The model predicts both the average grain size and distribution of grain size. The list of DN is analyzed regarding the grain size and the frequency of occurrence is calculated for every class of sizes.

In this work the model is enriched with the module that allows tracking of the selected phenomena in the CA cells, such as: occurring of nucleus, change of assignment to the grain, change of recrystallization level (i.e. how many times the recrystallization occurred in the volume represented by CA cell) and change of assignment to recrystallization cycle. The latter term is important in the further work and is explained below. The counter C represents recrystallization cycle and enables evaluation of recrystallized fraction of every cycle. Let's assume that at every CA cell in the initial microstructure has a counter $C = 0$. Any nucleus, which appears in the matrix of counter C, is marked with $C \leftarrow C + 1$. Any cell, which joins the grain with counter C is also marked with C. In consequence, the counter C represents the generation of the grain and consecutive generations could coexist in the material. In the further part of the work the term "recrystallization cycle" means rather "belonging to the generation C" than "material fully recrystallized C times". It is difficult to distinguish the grains belonging to various recrystallization cycles in experiments. Instead, the experimental data frequently refer to the term of recrystallized fraction, which combines recrystallized grains belonging to various cycles. Due to additivity of recrystallized fractions for the coexisting

cycles, the effective fraction of recrystallized material is obtained from the model.

3. Results

Several calculations were performed to assess the capabilities of the model. The attention was paid to evaluate the appropriateness of the connections between various outputs of the model, describing different aspects of the model behaviour. The applicability of the model is constrained by the assumptions described in previous part of the paper. It should be noted, however, that the results do not refer to any particular material. Instead, the presented results show the abilities of the model to reproduce some class of material responses or to meet some criteria.

Two types of materials were considered. The first is characterized by multi-peak flow stress curve (pure copper is a typical example). According to the Sakai structural criterion [18], an average grain size before process D_0 is related to grain size D after process as $2D > D_0$. The opposite criterion $2D < D_0$ is formulated for materials characterized by single peak on the flow stress curve, which are the second group of considered materials.

The calculations were performed for nominal temperature 1000°C and strain rate $1s^{-1}$. The simulated samples were of radius 4 mm and height 12 mm. The process was performed to the nominal strain of 0.67. The friction coefficient between the sample and the tool was 0.05.

3.1. Multi-peak flow stress behaviour

The fraction of material belonging to consecutive recrystallization cycles is shown in Fig. 3. The total recrystallized fraction is denoted with dashed line. The coexisting recrystallization cycles are observed in the material. Every cycle, except the first one, starts approximately at the inflection point of the curve for the previous one. The multi-peak flow curve obtained from the model is presented in Fig. 4a while idealized flow stress curve, taken from paper [22], is shown in Fig. 4b. The effective recrystallization fractions are also drawn in these figures. In comparison to Fig. 3b, the flow curve presented in Fig. 4a is characterized by smaller amplitude and regularity of the secondary peaks. However, good similarity of both the flow stress and recrystallization fraction is observed in Fig 4. The most distinctive points on these curves are marked. In both cases $x_{\mathrm{rec}} = 0.98$ is achieved at the beginning of the second oscillation. The oscillations observed on the curve are closely related to the curves denoting recrystallization fractions. Every recrystallization cycle calculated by the model starts approximately at the end of the previous cycle. This behaviour is confirmed by the results in Fig. 4b.

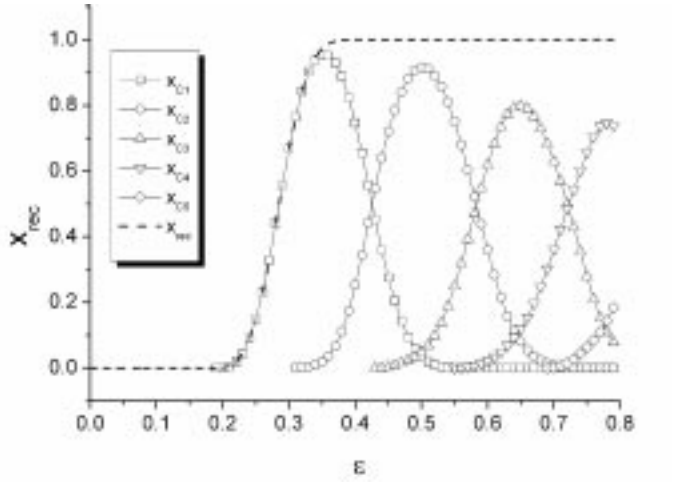

Fig. 3. Fraction of material belonging to the consecutive recrystallization cycles C=1 to C=5. Dashed line denotes the total recrystallization fraction

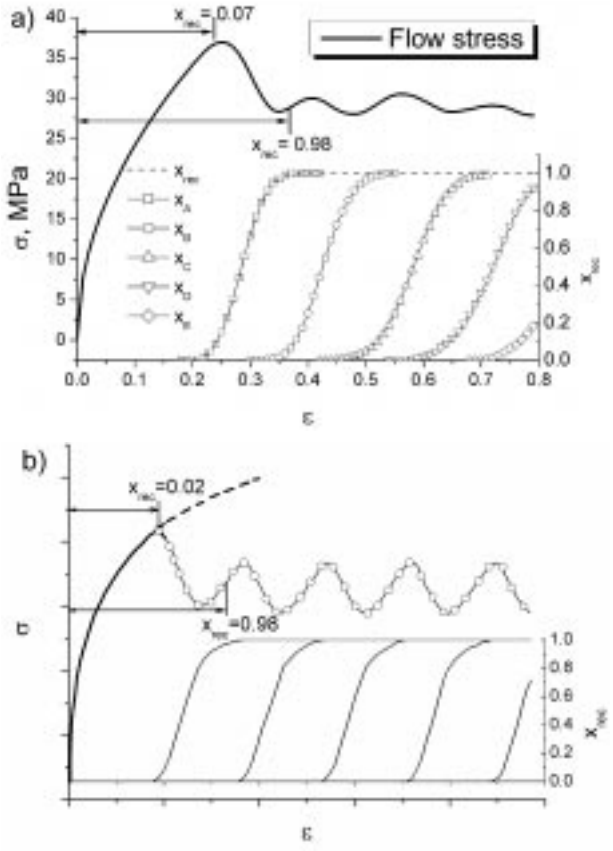

Fig. 4. Flow stress and recrystallization fraction: a) obtained from the model and b) idealized data (without units), based on [22]

Average grain size was calculated during the deformation (Fig. 5). The line of $D_0/2$ is drawn on the plot and it is seen the results obey the structural criterion in [18]. The relation between flow stress and average grain size is observed. While the overall tendency indicates decrease

of D, the local oscillations are revealed, which coincide with the peaks on the flow curve. The multi-peak flow stress curve is often accompanied with grain growth. The distributions of grain size in the material are tracked during simulation of deformation process. The results for selected strains are shown in Fig. 6. It is seen that at the strain corresponding to finish of the peak on flow curve (Fig. 4a), the microstructure consists of large amount of small and medium grains. However, there are also grains coarser than those observed in the initial microstructure, which is the evidence of grain growth. The first peak on the flow curve (Fig. 4a) contributes the coarse grains to the microstructure (Fig. 5 and Fig. 6b). The overall effect of increasing number of small and medium grains is seen in Fig. 5 and Fig. 6c,d, but the grain size distributions for consecutive strain steps show that the coarse grains are preserved. On the other hand, the recrystallized fraction shown in Fig. 4a suggests that the coarse grains are continuously rebuilt, because the DRX is still in progress. Thus, the onset of every DRX cycle is preceded by the growth of the grains nucleated in foregoing cycle. This leads in turn to the growth of the selected grains, which are unstable and will be replaced in the subsequent cycles.

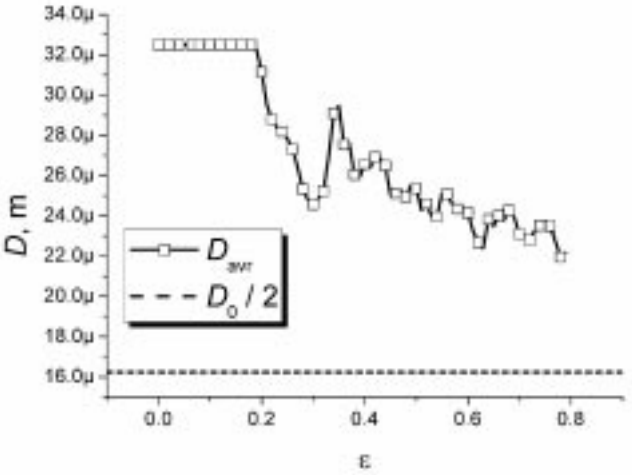

Fig. 5. Average grain size in the sample for multipeak flow stress material

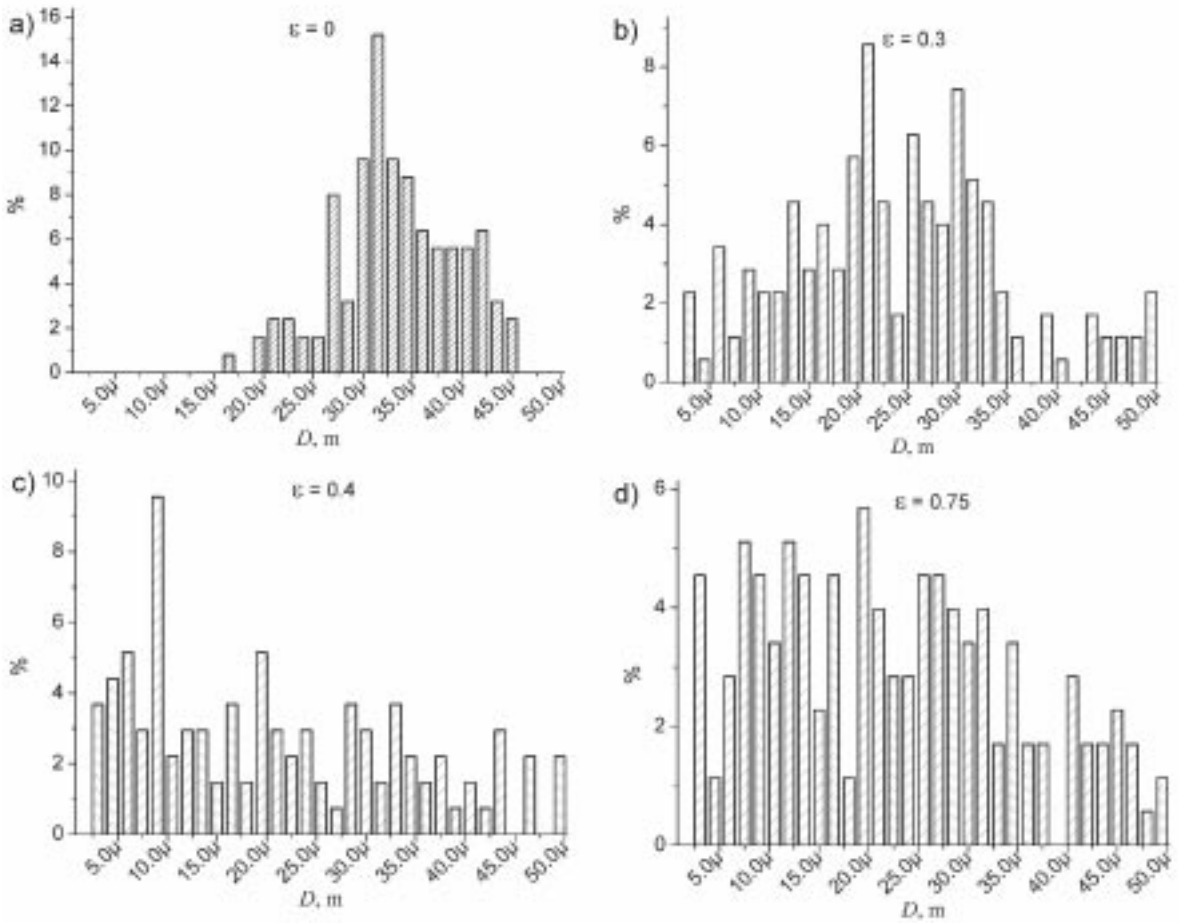

Fig. 6. Distribution of grain size for various strains: a) $\varepsilon = 0$, b) $\varepsilon = 0.3$, c) $\varepsilon = 0.4$, d) $\varepsilon = 0.75$

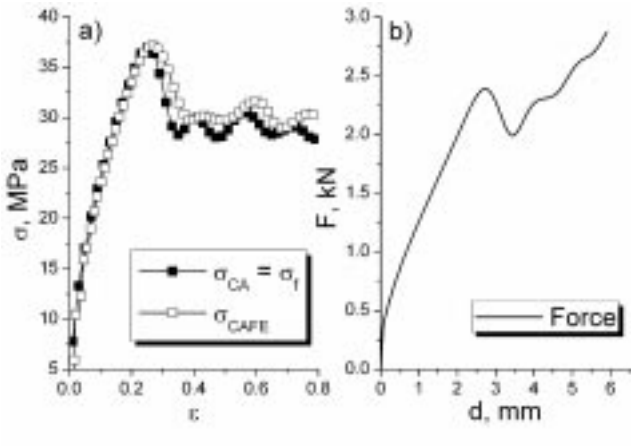

Fig. 7. The results obtained from macroscopic part of the coupled model: a) comparison between average stress calculated by CAFE (open symbols) and flow stress obtained from the stan-dalone CA model (filled symbols), b) compression force calculated by coupled CAFE model

The comparison between average stress obtained from the CAFE model and flow stress calculated by stan-dalone CA model is presented in Fig. 7a. The discrepancies in that figure are due to assumption of constant strain rate and temperature during the the CA calculation. The compression force calculated by CAFE model is shown in Fig. 7b. The results confirm the abilities of the model to describe the macroscopic behaviour of the deformed material.

3.2. Single-peak flow stress behaviour

The recrystallized fractions belonging to consecutive cycles are shown in Fig. 8. The comparison of the flow stress behaviour obtained from the model and idealized one, taken from [22], is presented in Fig. 9. It is seen in Fig. 8 that the grains of the second cycle appear almost at the same time as the grains of the first cycle. This suggests that the growth of the newly recrystallized grains is inhibited by the fast nucleation on their boundaries, what is source of the necklace structure [23]. The strong competition between consecutive cycles is also observed up to the fifth cycle. This can be caused by the grain refinement, see Fig. 10f. The cycles become regular above the strain of 0.4, which corresponds to the steady state on the flow stress curve (Fig. 9a). The onset of DRX, marked with $x_{\mathrm{rec}} = 0.05$, is more distinct for the data calculated form the model. Fig. 9a and 9b reveal good agreement between predicted value of recrystallization fraction $x_{\mathrm{rec}} = 0.98$, which is observed in both cases at the finish of the peak on the flow stress curve. The steady state flow stress in Fig. 9a consists of multiple small oscillations, which are also observed in Fig. 9b. The effective recrystallized fraction curves in Fig. 9a are connected with the oscillations on the flow stress curve. It should be also pointed out that every effective recrystallized fraction curve, except the first one, starts approximately at the inflection point of the curve describing previous cycle. Thus, the recrystallization cycles overlap each other.

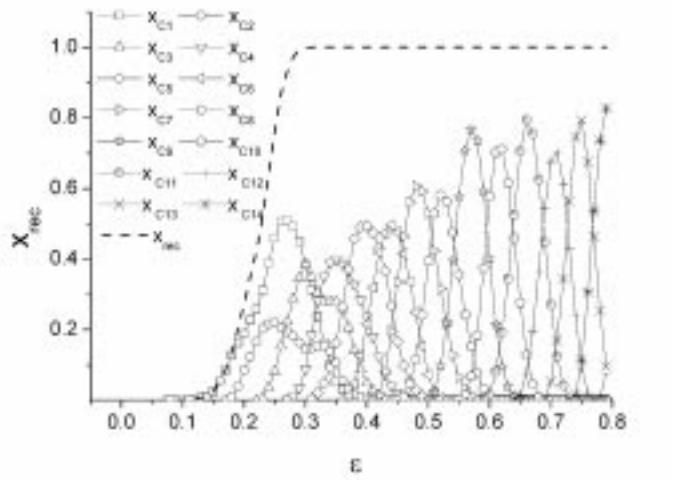

Fig. 8. Fraction of material belonging to the coexisting recrystallization cycles. The indexes C1 to C14 represents the recrystallized volume fractions for consecutive cycles. Dashed line denotes the total recrystallized volume fraction

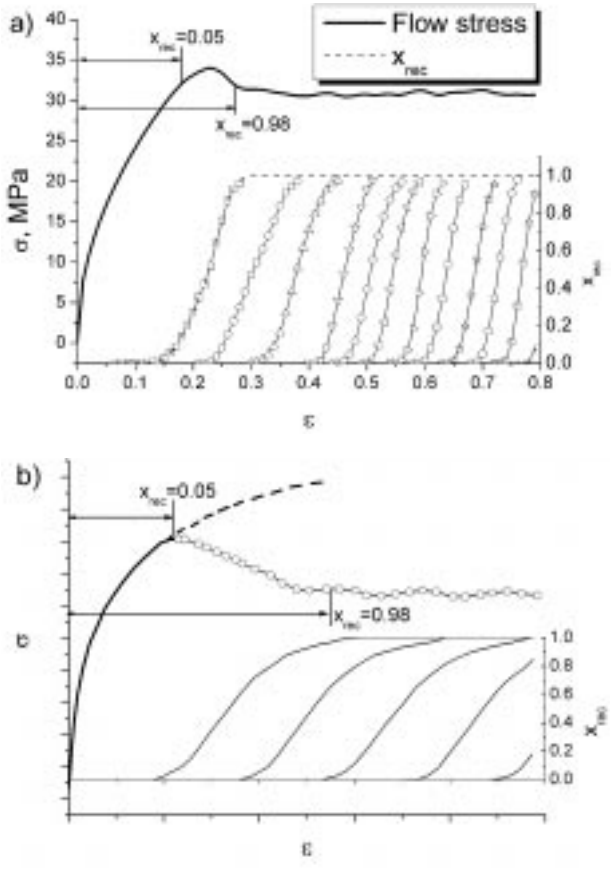

Fig. 9. Flow stress and recrystallized volume fraction: a) obtained from the model and b) idealized data (without units), based on [22]

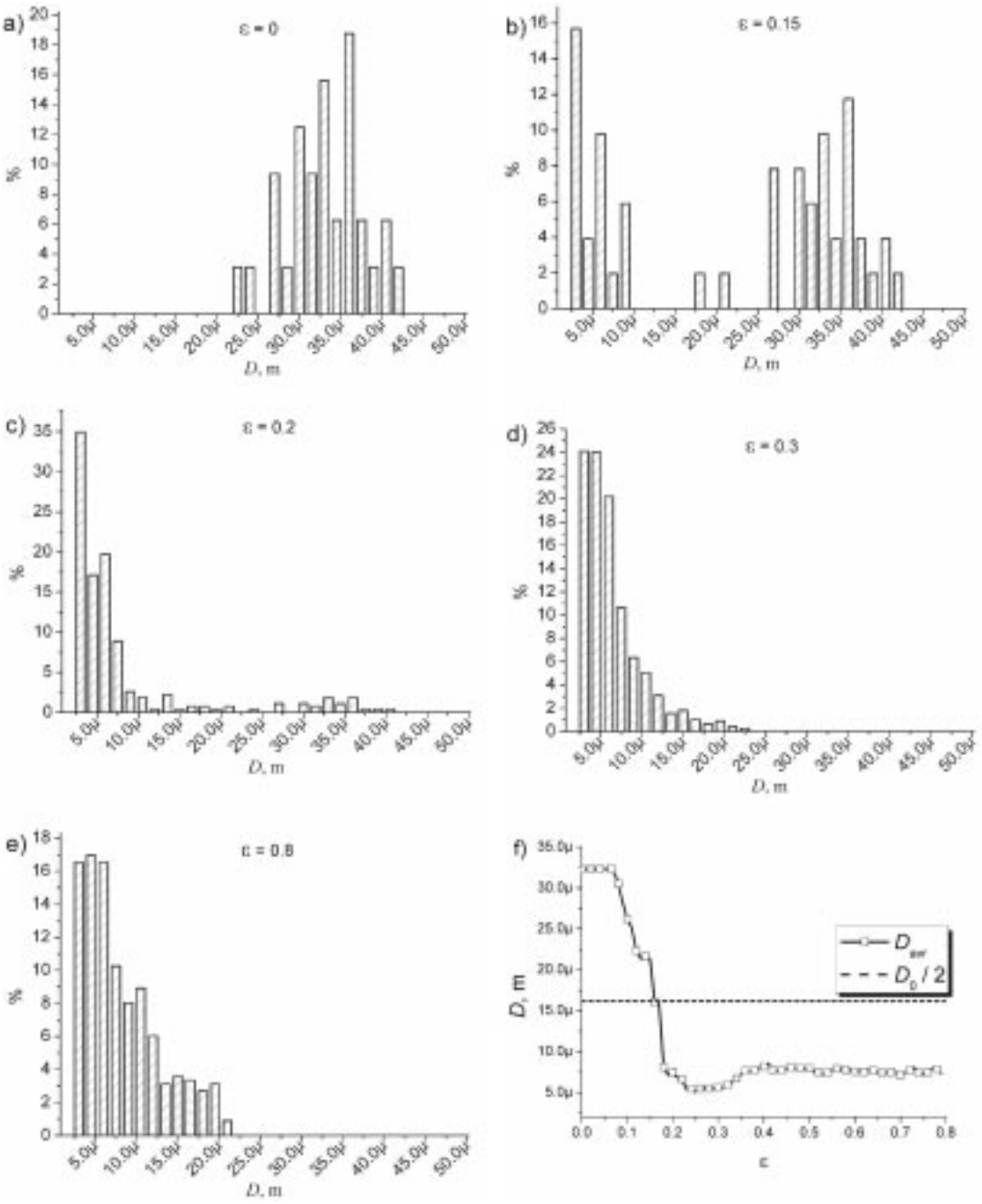

Fig. 10. Distribution of grain size for various strains: a) $\varepsilon = 0$, b) $\varepsilon = 0.15$, c) $\varepsilon = 0.2$, d) $\varepsilon = 0.3$ e) $\varepsilon = 0.8$ and f) plot of average grain size in the sample

The grain size distribution during the deformation is shown in Fig. 10a-e and the average grain size is presented in Fig. 10f. The initial-to-final grain size ratio is greater than 2 according to Sakai structural criterion. The grain refinement is observed during deformation and the finest average grain size are obtained for $\varepsilon \approx 0.25$. Steady grain size is observed for $\varepsilon > 0.4$. Comparison of Fig. 10d and 10e reveals that final grains are coarser than those at the end of the peak on flow curve.

3.3. Discussion

Despite the model predicts the distribution of grain size, the volume fraction of ultra small grains seems to be overestimated. This artefact of the model results from the assumption that nucleus has to be a whole CA cell. Since the cell is indivisible, the whole area of the cell is taken in equation (6), which leads to inaccuracy of the grain size distribution. The more nuclei appear in the CA lattice, the more intensive is this negative effect.

The overestimation of nuclei size is seen at the curves of average grain size, as well. However, the structural criterion of [18] is still satisfied. Thus, it is possible to conclude that this source of inaccuracy should be respected, but its influence does not affect the results to the large extent.

The model offers subtle insight into mechanism of dynamic recrystallization. The coexisting cycles of recrystallization are distinguishable, which is important for the analysis. In comparison to the phenomenological models, which use the percentage of recrystallization as the only measure of DRX progress, this model provides a substantial improvements. The percentage of DRX reaches 100% for relatively low values of strain, despite the process of DRX continues for larger strains. The value of recrystallized fraction obtained from the model seems to be more adequate to describe the actual progress of DRX. The model is able to predict the distribution of grain size. It should be emphasized that the calculated distributions result from the model behaviour and are not directly given by phenomenological equations.

4. Conclusions

The microscale CA model provides some improvements in comparison to those already published (e.g. [6-10]). The consistency with the theory of cellular automata is improved by the concept of the distant neighbourhood and elimination of nucleation rate (or nucleation probability) model. To the knowledge of the authors, the idea of keeping the track of the grains belonging to different DRX cycles was not presented before in DRX models based on CA. The mutual feedback between CA and FE simulation which provides nonuniform strain rates and temperature to the CA model, is another advantage of the present approach. The FE method is supported by simulation of microstructure development, which enables accounting for nondeterministic phenomena and non-continuous regions inside material, e.g. grain boundaries. On the other hand, inhomogeneities of strain rate and temperature, calculated by the FE, influence the progress of CA simulation of DRX. Eventually, the integrated CAFE model provides information about both thermo-mechanical and microstructural properties of the material for massive samples.

Acknowledgements

The financial support of MNiSzW, project no. 11.11.110.643 is gratefully acknowledged.

Received: 10 February 2007.

REFERENCES

[1] A. Rollett, Prog. Mat. Sci. **42**, 79-99 (1997).
[2] M. A. Miodownik, J. Light Metals **2**, 125-135 (2002).
[3] C. Roucoules, M. Pietrzyk, P.D. Hodgson, Mat. Sci. Eng. **A339**, 1-9 (2003).
[4] H. Ahmed, M.A. Wells, D.M. Maijer, B.J. Howes, M.R. van der Winden, Mat. Sci. Eng. **A390**, 278-290 (2005).
[5] C. H. J. Davies, Scr. Mater. **36**, 35-40 (1997).
[6] R. Ding, Z. Guo, Acta Mater. **49**, 3163-3175 (2001).
[7] J. Kroc, Simulation of Dynamic Recrystallization by Cellular Automata. PhD thesis, Mathematical and Physical Faculty of Charles University, Prague (2001).
[8] M. Qian, Z.X. Guo, Mat. Sci. Eng. **A365**, 180-185 (2004).
[9] G. Kugler, R. Turk, Acta Mater. **52**, 4659-4668 (2004).
[10] J. Gawąd, L. Madej, D. Szeliga, M. Pietrzyk, Act. Met. Slov. **11**, 45-53 (2005).
[11] N. Yazdipour, C.H.J. Davies, P.D. Hodgson, Computer Methods in Materials Science **7**, 168-174 (2007).
[12] S. Das, E.J. Palmiere, I.C. Howard, CAFE: Proc. Thermomech. Processing: Mechanics, Microstructure & Control, eds, E.J. Palmiere, M. Mahfouf, C. Pinna, Sheffield, 296-301 (2002).
[13] A. Shterenlikht, 3D CAFE Modeling of Transitional Ductile – Brittle Fracture in Steels. PhD thesis, Univeristy of Sheffiled, (2003).
[14] J. G. Lenard, M. Pietrzyk, L. Cser, Mathematical and Physical Simulation of the Properties of Hot Rolled Products, Elsevier, Amsterdam (1999).
[15] Y. Liu, T. Baudin, R. Penelle, Scripta Mater. **34**, 1679-1683 (1996).
[16] C.H.J. Davies, Scripta Metal. Mater. **33**, 1139-1143 (1995).
[17] H. Mecking, U.F. Kocks, Acta Metall. **29**, 1865-1875 (1981).
[18] T. Sakai, J. Mat. Proc. Techn. **53**, 349-361 (1995).
[19] W. Roberts, B. Ahlblom, Acta Metall **29**, 801-813 (1978).
[20] F. J. Humphreys, Acta Mater. **45**, 4231-4240 (1997).
[21] M. Winning, G. Gottstein, L. S. Shvindlerman, Acta Mater. **50**, 353-363 (2002).
[22] R. M.J. Luton, C.M. Sellars, Acta Metall. **17**, 1033-1044 (1969).
[23] D. Ponge, G. Gottstein, Acta Mater. **46**, 69-80 (1998).